Neoplasia 62 (2025) 101146

Contents lists available at ScienceDirect

Neoplasia

journal homepage: www.elsevier.com/locate/neo

Original Research

Exogenous BMI1 expression aggravates oral squamous cell carcinomas in tongue epithelia

Jorge Baquero [a,b], Xiao-Han Tang [a,b], Daniel Galke [a,c], Theresa Scognamiglio [d], Tuo Zhang [e], Dawson Miller [a], Qiuying Chen [a], Steven Gross [a], Lorraine J. Gudas [a,b,c,*]

[a] Department of Pharmacology, Weill Cornell Medical College, New York, NY, USA
[b] Meyer Cancer Center, Weill Cornell Medicine, New York, NY, USA
[c] Department of Pharmacology, Weill Cornell Graduate School of Biomedical Sciences, New York, NY, USA
[d] Department of Pathology, Weill Cornell Medical College, New York, NY, USA
[e] Genomics Resources Core Facility, Weill Cornell Medical College, New York, NY, USA

ARTICLE INFO

Keywords:
Epigenetics
Oral squamous cell carcinoma
HIF1α
Metabolic reprogramming
SOX9
Transcriptional regulation

ABSTRACT

Oral squamous cell carcinoma (OSCC) is characterized by aggressiveness and a poor prognosis, in part because most patients are diagnosed during the later stages of the disease. B cell-specific Moloney murine leukemia virus integration site 1 (BMI1), part of polycomb repressive complex 1 (PRC1), is a key transcription factor overexpressed in OSCC. Although increased BMI1 has been linked to tumor formation in mouse models of the disease, the molecular mechanisms have not been elucidated. Here we used a transgenic mouse line (KrTB) that selectively overexpresses BMI1 in the tongue basal epithelial stem cells (SCs) to delineate BMI1 actions during oral tumorigenesis. By tumor pathological classification after 4-nitroquinoline 1-oxide (4-NQO)-induced carcinogenesis we detected more severe tumors in mice with ectopic BMI1 expression. Genome-wide transcriptomics indicated that mRNAs associated with human OSCC, including SOX9, HIF1A, MMP9, INHBB, and MYOF, were further increased by ectopic BMI1 expression in murine tongue epithelia. mRNAs encoding multiple metabolic targets, such as SLC2A1 (GLUT1), PKM, LDHA, and HK2, were also increased upon BMI1 overexpression in 4-NQO-treated tongue epithelia. Furthermore, we detected BMI1, SOX9, and GLUT1 proteins in the infiltrating cells of invasion fronts identified by markers of invasive SCCs. Finally, metabolomic data show that BMI1 overexpression in tongue epithelia promotes glycolysis during 4-NQO-induced carcinogenesis. Thus, our data demonstrate that BMI1 causes OSCC cells to alter cell metabolism, as changes in many of these transcripts are linked to increased glycolysis and metabolic reprograming that occurs during carcinogenesis.

Significance

Tumor aggressiveness and invasive lesions are common hallmarks of late stages of oral squamous cell carcinomas (OSCC). Unfortunately, the majority of OSCC diagnoses occur in these advanced stages of the disease. Our data indicate that BMI1 overexpression, as reported in human patient samples, increases the severity of oral tumors in an OSCC murine model by increasing the percentages of invasive lesions. We demonstrate that BMI1 overexpression changes cellular metabolism by promoting glycolysis during oral tumorigenesis, an important feature of human cancers. These results could potentially lead to new therapies for OSCC patients with limited options, complementing current strategies used to treat advanced oral cancers.

Introduction

Head and neck squamous cell carcinomas (HNSCCs), which include

Abbreviations: 4-NQO, 4-nitroquinoline 1-oxide; BMI1, B cell-specific Moloney murine leukemia virus integration site 1; ChIP, chromatin immunoprecipitation; CSCs, cancer stem cells; DOX, doxycycline; HIF1A, hypoxia inducible factor 1 subunit alpha; HNSCC, head and neck squamous cell carcinoma; IF, immunofluorescence; IHC, immunohistochemistry; Kr, K14-rtTA mice; KrTB, K14-rtTA;TRE-FLBmi-1 mice; OSCC, oral squamous cell carcinoma; PRC1, polycomb repressive complex 1; RNA-seq, RNA sequencing; SCs, stem cells; SCC, squamous cell carcinoma; SOX9, SRY-box transcription factor 9.

* Corresponding author at: E409, Weill Cornell Medicine, 1300 York Avenue, New York, NY 10065, USA.
E-mail address: ljgudas@med.cornell.edu (L.J. Gudas).

https://doi.org/10.1016/j.neo.2025.101146
Received 27 January 2025; Received in revised form 18 February 2025; Accepted 18 February 2025

cancers of the oral cavity, pharynx, and esophagus, represent the seventh most common cancer in the world [1]. In the US alone, the American Cancer Society reports that 58,450 new cases of oral cavity and pharynx cancers and 12,230 related deaths are expected in 2024 [2]. While 5-year survival rates for HNSCC have increased moderately in the last decades, most patients are diagnosed during later stages and require treatments consisting of surgery followed by chemoradiotherapy or immunotherapy [3–5]. Current efforts are aimed at the identification of potential biomarkers and therapeutic targets [3,5], which demands a broader understanding of the molecular biology of this disease.

B cell-specific Moloney murine leukemia virus integration site 1 (BMI1) is a key transcription factor overexpressed in oral squamous cell carcinomas (OSCC), a type of HNSCC [6–8]. BMI1 is a member of the mammalian Polycomb Repressive Complex (PRC1), and one function of this complex is the ubiquitination of histone H2A to repress target gene expression [9]. PRC1-regulated genes are involved in processes such as stem cell self-renewal, cell differentiation, and proliferation [10,11]. Although BMI1 itself does not contain E3 ubiquitin ligase activity and must form a complex with other PRC1 members to ubiquitinate H2AK119 [12], studies indicate that BMI1 can also function independently of PRC1 [13,14].

BMI1 is expressed in almost all tongue basal stem cells (SCs) [15], which divide asymmetrically to give rise to all progeny cells that differentiate and maintain this epithelial layer [16]. Consequently, cell clusters in tongue epithelia that are derived from single, BMI1-labeled SCs are visible 13 months after labeling [15]. Using lineage tracing in our previously developed mouse model of HNSCC in which tumors are induced by the tobacco-surrogate and carcinogen 4-nitroquinoline 1-oxide (4-NQO) [17], we reported that labeled basal SCs are present in papillomas and invasive squamous cell carcinomas and that these SCs are the cells of origin of tongue tumors [18]. These cancer stem cells (CSCs) are BMI1-positive and can give rise to entire regions in developing tumors in a mouse model of HNSCC [7], driving invasive growth and metastasis [19]. Furthermore, we previously developed a transgenic mouse line (KrTB) that expresses ectopic BMI1 selectively in tongue basal epithelial SCs only upon doxycycline (DOX) treatment and we showed that high, *exogenous* BMI1 expression in basal SCs enhances tumor formation upon 4-NQO treatment in the HNSCC model [20]. Here, we use this KrTB line to elucidate the molecular signals by which high, ectopic BMI1 expression increases the severity of OSCC.

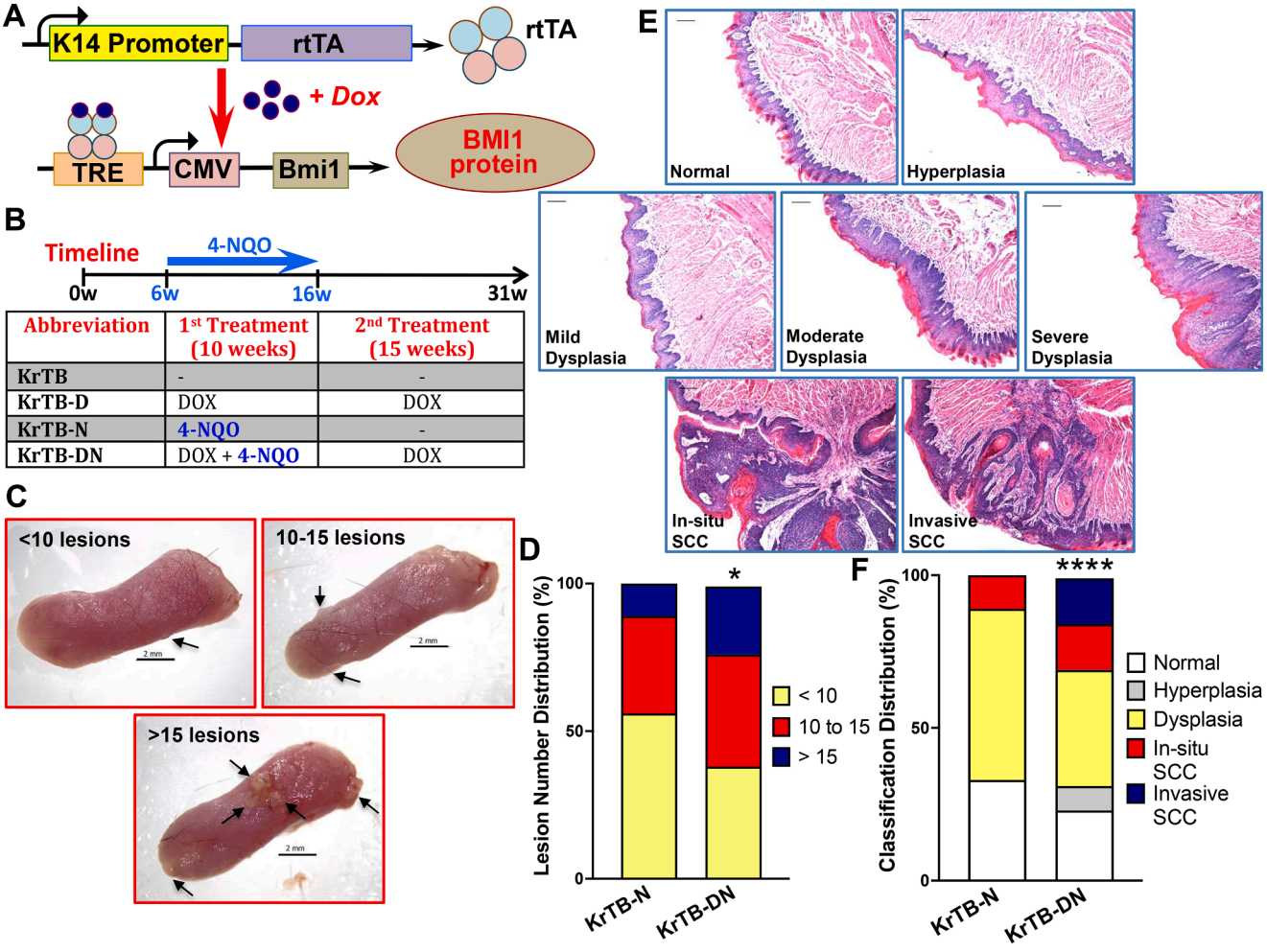

Abbreviation	1st Treatment (10 weeks)	2nd Treatment (15 weeks)
KrTB	-	-
KrTB-D	DOX	DOX
KrTB-N	4-NQO	-
KrTB-DN	DOX + 4-NQO	DOX

Fig. 1. Tumor pathological classification after 4-NQO-induction reveals more severe lesions in mice with ectopic BMI1 expression (KrTB-DN mice). (**A**) Schematic illustrating the doxycycline-inducible ectopic BMI1 expression system in KrTB transgenic mice. (**B**) Timeline outlining the different treatment groups for this experiment. All samples were collected at 31 weeks. (**C**) Representative whole tongue images displaying varying numbers of visible lesions from 4-NQO treated mice (10X magnification; 2mm scales bar). Arrows highlight tongue lesions and progression with increasing number. (**D**) Graph of the distribution (%) of tongue lesions by lesion number from KrTB-N ($N = 9$) and KrTB-DN ($N = 13$) mice. (**E**) Representative images of H&E stained sections for normal tongue epithelium, hyperplasia, dysplasia, in-situ squamous cell carcinoma (in-situ SCC), and invasive SCC (100X magnification; 100 μm scale bar). (**F**) Distribution of the most severe 4-NQO-induced lesion observed in each mouse by pathological classification, with KrTB-N ($N = 9$) and KrTB-DN ($N = 13$) mice. For **D** and **F**, statistical significance was determined with the chi-square test. *0.01<p<0.05, **0.001<p<0.01, ***0.0001<p<0.001, ****p<0.0001.

Results

Tumor pathological classification after 4-NQO-induced carcinogenesis reveals more severe lesions in mice with ectopic BMI1 expression

Here we used the transgenic (KrTB) mouse line in which ectopic, FLAG-tagged BMI1 is overexpressed in the stem cells (SCs) of tongue epithelia [20,21]. This line contains a reverse tetracycline-controlled transactivator (rtTA) driven by a truncated human keratin 14 promoter (Fig. 1A). In the presence of doxycycline (DOX), rtTA binds to the tetracycline response element (TRE) upstream of the FLAG-BMI1 sequence. Therefore, we can increase BMI1 protein expression in epithelial SCs with DOX in the drinking water (labeled as KrTB-D) (Fig. 1A). We used the KrTB transgenic line in our immunocompetent mouse model of OSCC [17,22] to characterize the actions of BMI1 during carcinogenesis. Our model uses the carcinogen 4-nitroquinoline 1-oxide (4-NQO) to induce oral cavity cancer in mice, simulating many aspects of human OSCC [23,24]. All experimental groups are defined in Fig. 1B.

We first assessed the severity of OSCC by counting visible tongue lesions in 4-NQO treated mice (KrTB-N and KrTB-DN groups, Fig. 1B) in a blinded manner [20,22]. Representative images of tongues with varying numbers of visible lesions are shown (Fig. 1C). We found higher percentages of mice with greater than 15 lesions in the KrTB-DN (23.1 %, $P = 0.018$) compared to the KrTB-N group (11.1 %) (Fig. 1D). Next, we evaluated H&E sections and classified the most severe tongue lesion in each 4-NQO treated tongue (KrTB-N and KrTB-DN groups, Fig. 1B). Premalignant and malignant lesions were classified as hyperplasia, dysplasia (mild, moderate, and severe), in situ SCC, or invasive SCC (Fig. 1E) by a board certified pathologist (T.S.) [20,22]. We identified the most aggressive type of lesion (invasive SCCs) only in mice with ectopic BMI1 expression (KrTB-DN group, 15 %, $P < 0.0001$) (Fig. 1F). In contrast, in-situ SCCs (11 %) were the most severe lesions identified in the KrTB-N group.

Transcripts associated with OSCC are further increased by ectopic BMI1 expression in tongue epithelia

We assessed the effects of ectopic BMI1 overexpression under both normal conditions and with 4-NQO treatment by performing genome-

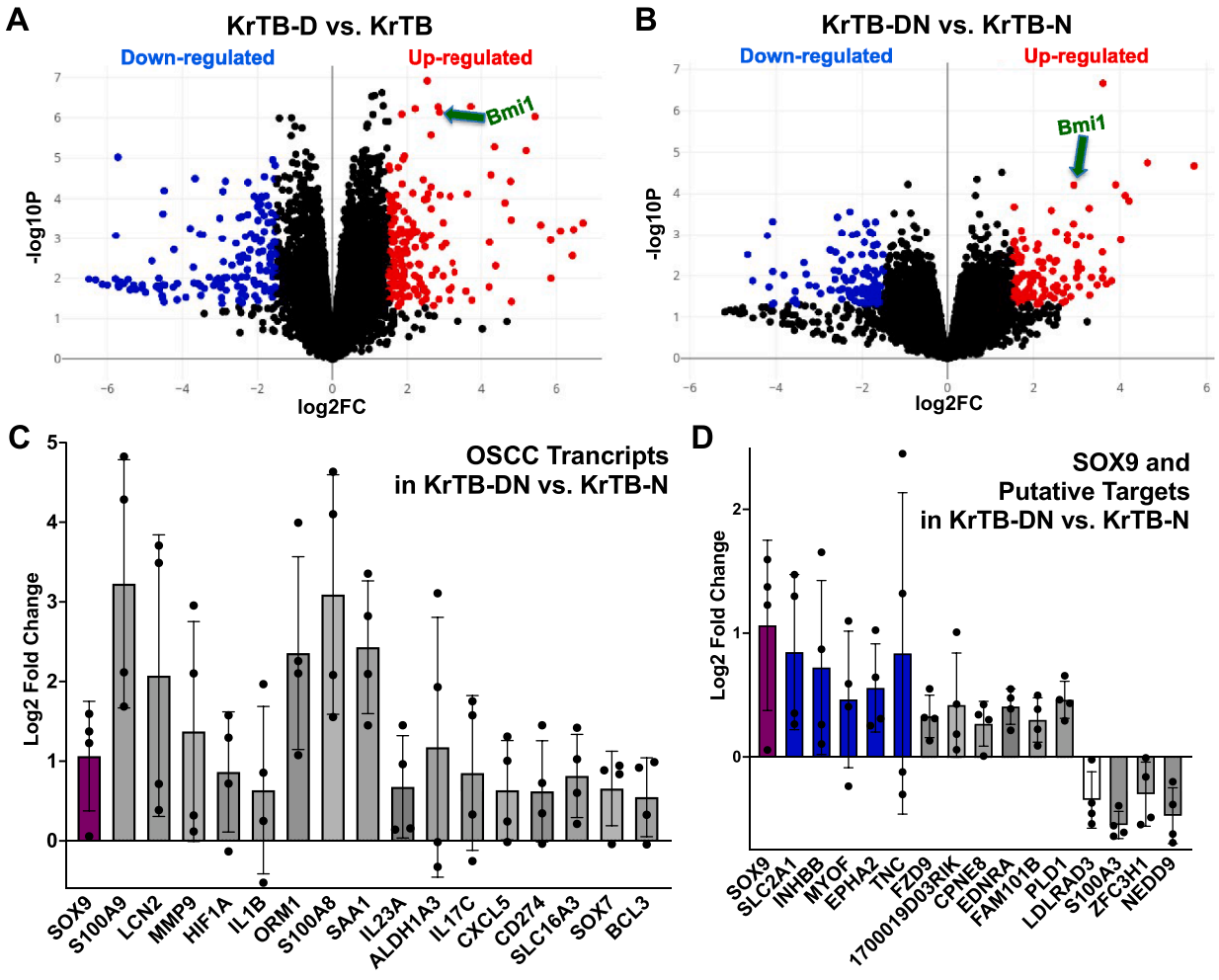

Fig. 2. RNA sequencing indicates the transcripts that are differentially expressed in KrTB-D vs. KrTB, and in KrTB-DN vs. KrTB-N tongue epithelia. (**A-B**) Volcano plots displaying the log2-fold changes and statistical significance of each transcript calculated by performing differential gene expression analyses from (**A**) KrTB-D ($N = 4$) vs. KrTB ($N = 4$), and from (**B**) KrTB-DN ($N = 4$) vs. KrTB-N ($N = 4$) tongue epithelia (adjusted p-value <0.1). Every point in the plots represents a transcript. Red points indicate significantly upregulated transcripts, blue points indicate downregulated transcripts. These plots were generated using BioJupies (Ma'ayan Lab, Icahn School of Medicine at Mount Sinai). (**C**) Fold change of gene expression levels of SOX9 (in purple) and other 4-NQO-induced targets in KrTB-DN vs. KrTB-N tongue epithelia. (**D**) Fold change of gene expression levels of SOX9 (in purple) and SOX9 putative targets in KrTB-DN vs. KrTB-N tongue epithelia. mRNA targets that are also 4-NQO-induced in WT mice are depicted in blue. For (C) and (D), data graphed denotes the mean ± standard deviation of the mean (SD).

wide RNA sequencing (RNA-seq) analyses on tongue epithelia. First, we compared groups treated ± DOX (KrTB-D vs. KrTB) but not 4-NQO (Fig. 1B) and identified 2591 transcripts that were increased and 2056 transcripts that were decreased in the KrTB-D compared to the KrTB group ($P < 0.05$) (Fig. 2A, Sup. Table 1). By Gene Ontology enrichment and KEGG pathway analyses we found that the most significantly increased biological processes and pathways (Sup. Fig. 1A-B) were extracellular matrix (ECM) organization, ECM-receptor interaction, focal adhesion, regulation of cell motility, and regulation of cell migration. Skin development was the only biological process that was significantly decreased upon BMI1 overexpression (Sup. Fig. 1A-B).

We then evaluated the effects of BMI1 overexpression with 4-NQO treatment (KrTB-DN vs. KrTB-N, Fig. 1B) and identified 1722 transcripts that were increased and 1093 transcripts that were decreased ($P < 0.05$) upon ectopic BMI1 expression (Fig. 2B, Sup. Table 2). Multiple phosphorylation and signaling pathways, as well as carboxylic acid transport, HIF-1 signaling, and central carbon metabolism in cancer were among the top upregulated processes and pathways with ectopic BMI1 overexpression in the presence of 4-NQO (Sup. Fig. 1C-D). Only two biological processes were significantly decreased with BMI1 overexpression in the presence of 4-NQO (Sup. Fig. 1C-D).

Analysis of WT mice demonstrated that treatment with 4-NQO is associated with increases in numerous transcripts linked to human OSCCs (Sup. Fig. 2A) [25]. Our RNA-seq data revealed that these 4-NQO induced transcripts were further increased in KrTB-DN compared to KrTB-N tongues (Fig. 2C). These transcripts include SOX9, a transcription factor associated with stem-like phenotypes in cells of oral tumors [26]. Chromatin immunoprecipitation (ChIP) of tongue epithelia from DOX treated and age-matched untreated KrTB mice [21] confirmed that BMI1 is associated with the promoter region of the SOX9 gene (Sup. Fig. 3). Multiple SOX9 putative target mRNAs reported in other types of stem cells [27] were elevated in tongues of 4-NQO-treated WT mice (in blue, Sup. Fig. 2B). These SOX9 putative targets were also further increased in KrTB-DN compared to KrTB-N tongue epithelia (in blue, Fig. 2D). These transcripts (SLC2A1, INHBB, MYOF, EPHA2, and TNC) have been linked to poor OSCC patient survival [28–32]. Thus, from our RNA-seq data, we suggest that ectopic BMI1 overexpression increases the severity of tongue tumors at least in part by further elevating the levels of these transcripts (Fig. 2C-D).

BMI1 overexpression in 4-NQO-treated tongue epithelia increases SOX9 and HIF1α proteins

As SOX9 and HIF1α proteins are elevated in human OSCC and are poor prognostic factors for this disease [26,33,34], we next investigated if SOX9 and HIF1α proteins are also increased in KrTB-DN mice. We performed immunohistochemistry (IHC) to quantify protein levels of BMI1, SOX9, HIF1α, and Ki67, a marker of actively proliferating cells, in tongue epithelia from all four experimental groups (Fig. 1B). As expected, BMI1 protein was expressed in basal SCs and suprabasal cells of

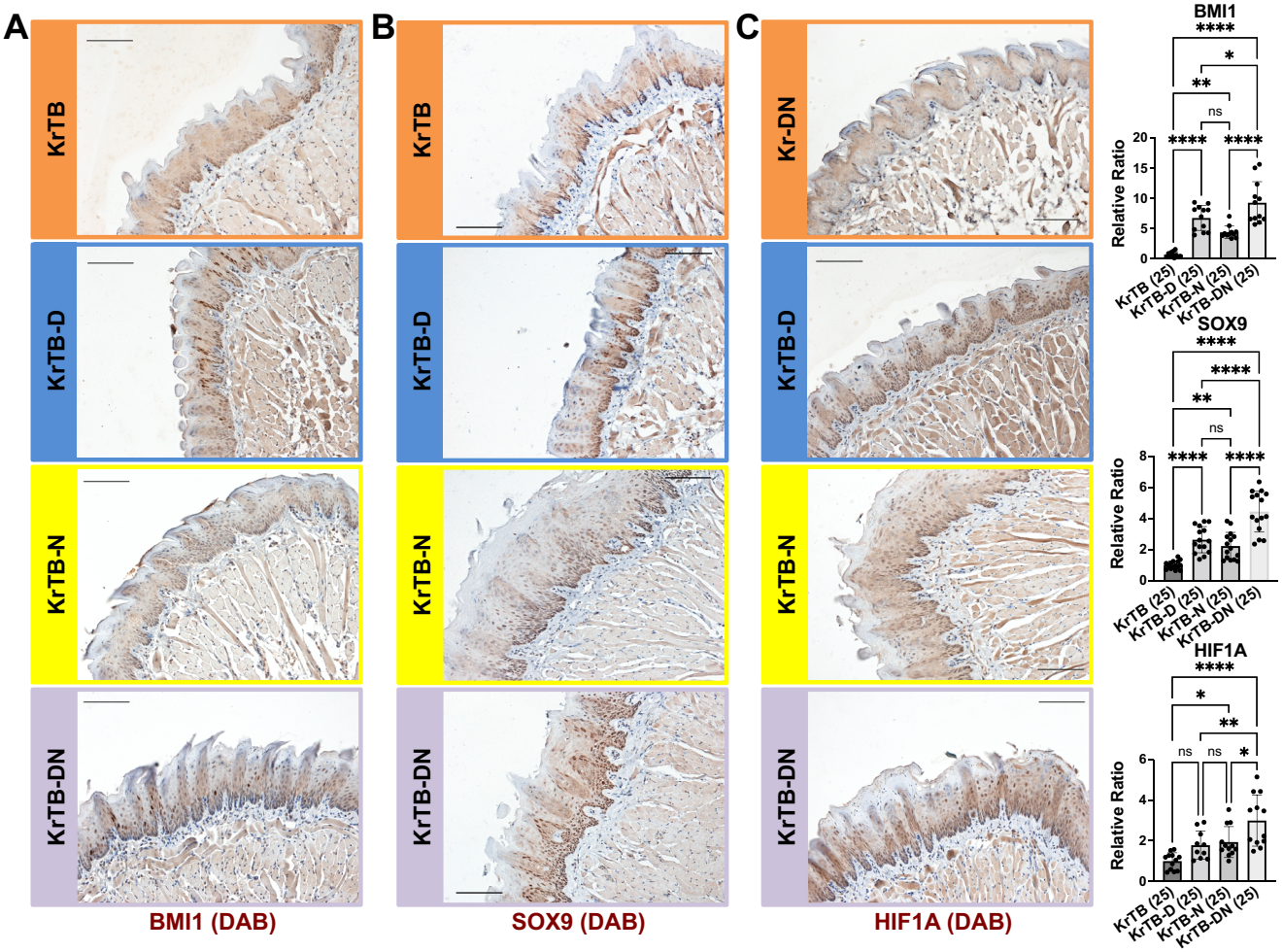

Fig. 3. BMI1 overexpression increases SOX9 and HIF1α expression in 4-NQO-treated tongue epithelia. (**A**) BMI1, (**B**) SOX9, and (**C**) HIF1α IHC stainings in KrTB, KrTB-D, KrTB-N and KrTB-DN tongue epithelia (200X; scale bar: 100 μm; $N = 3$ mice/group, 4-5 fields/mouse; representative fields are shown). Ratios of the levels of these proteins in all groups relative to levels in the KrTB group are also included. Data graphed denotes the mean ± standard deviation of the mean (SD). Statistical significance was determined using one-way ANOVA followed by Turkey's test. *0.01<p<0.05, **0.001<p<0.01, ***0.0001<p<0.001, ****p<0.0001.

tongue epithelia (KrTB, Fig. 3A) and levels were increased 6.7 fold upon DOX (KrTB-D) and 4.4 fold with 4-NQO treatment (KrTB-N). BMI1 protein levels were the highest in the KrTB-DN group (9.3 fold higher compared to KrTB, Fig. 3A).

As BMI1 is highly expressed in rapidly proliferating cells, such as cancer stem cells (CSCs) [19], we assessed Ki67 expression in all experimental groups. Ki67 is mainly expressed in the basal SCs of oral epithelia [22]. We show that Ki67 protein, compared to that of BMI1 protein, follows a similar trend, increasing upon DOX and 4-NQO treatments (KrTB-D and KrTB-N compared to KrTB, Sup. Fig. 4). Furthermore, Ki67 levels were the highest in KrTB-DN tongues (2.2 fold higher compared to KrTB, Sup. Fig. 4).

Next, we assessed SOX9 protein and confirmed that this protein is expressed in basal SCs and suprabasal cells of tongue epithelia (KrTB, Fig. 3B). SOX9 protein levels were increased 2.6 fold in KrTB-D and 2.2 fold in KrTB-N samples compared to the KrTB group (Fig. 3B). SOX9 levels were 4.4 fold higher in KrTB-DN compared to KrTB tongues (Fig. 3B). Thus, SOX9 protein, a 4-NQO-regulated target, was further increased with BMI1 overexpression (compare KrTB-DN vs. KrTB-N, Fig. 3B). Our IHC results identified SOX9 protein as a downstream target of BMI1 during oral carcinogenesis.

Additionally, we assessed HIF1α protein; HIF1α protein was detected in basal SCs and suprabasal cells and the levels were not increased by BMI1 overexpression (KrTB-D vs. KrTB, Fig. 3C). However, HIF1α protein levels were increased in KrTB-N vs. KrTB and further increased in KrTB-DN vs. KrTB-N tongues, Fig. 3C). Thus, while SOX9 expression is always increased when ectopic BMI1 is expressed, HIF1α protein is only increased upon ectopic BMI1 expression in the 4-NQO-treated tongues.

BMI1, SOX9, and GLUT1 proteins are detected in the infiltrating cells of invasion fronts identified by markers of invasive SCCs

We then focused on samples from 4-NQO-treated mice (KrTB-N and KrTB-DN, Fig. 1B). We stained for E-cadherin and CD44 proteins in the most severe lesions from both groups, as loss of E-cadherin (hallmark of epithelia-to-mesenchymal transition, EMT) and increased CD44 expression strongly correlate with more aggressive tongue tumors [35, 36]. BMI1, E-cadherin, CD44, and SOX9 were expressed in most basal SCs of normal oral epithelia and in *in-situ* SCC lesions of KrTB-DN (Fig. 4A) and KrTB-N mice (Sup. Fig. 5). Only KrTB-DN tongues exhibited invasive SCCs (see Fig. 1F), and an invasive lesion contained increased levels of BMI1, CD44, and SOX9, as well as lower levels of E-cadherin, compared to normal oral epithelia (Fig. 4A). We closely examined invasive fronts and identified cells that stained for BMI1, CD44, and SOX9 infiltrating underlying muscle tissue, (circled areas, Fig. 4A). A second invasive SCC lesion from a different KrTB-DN mouse

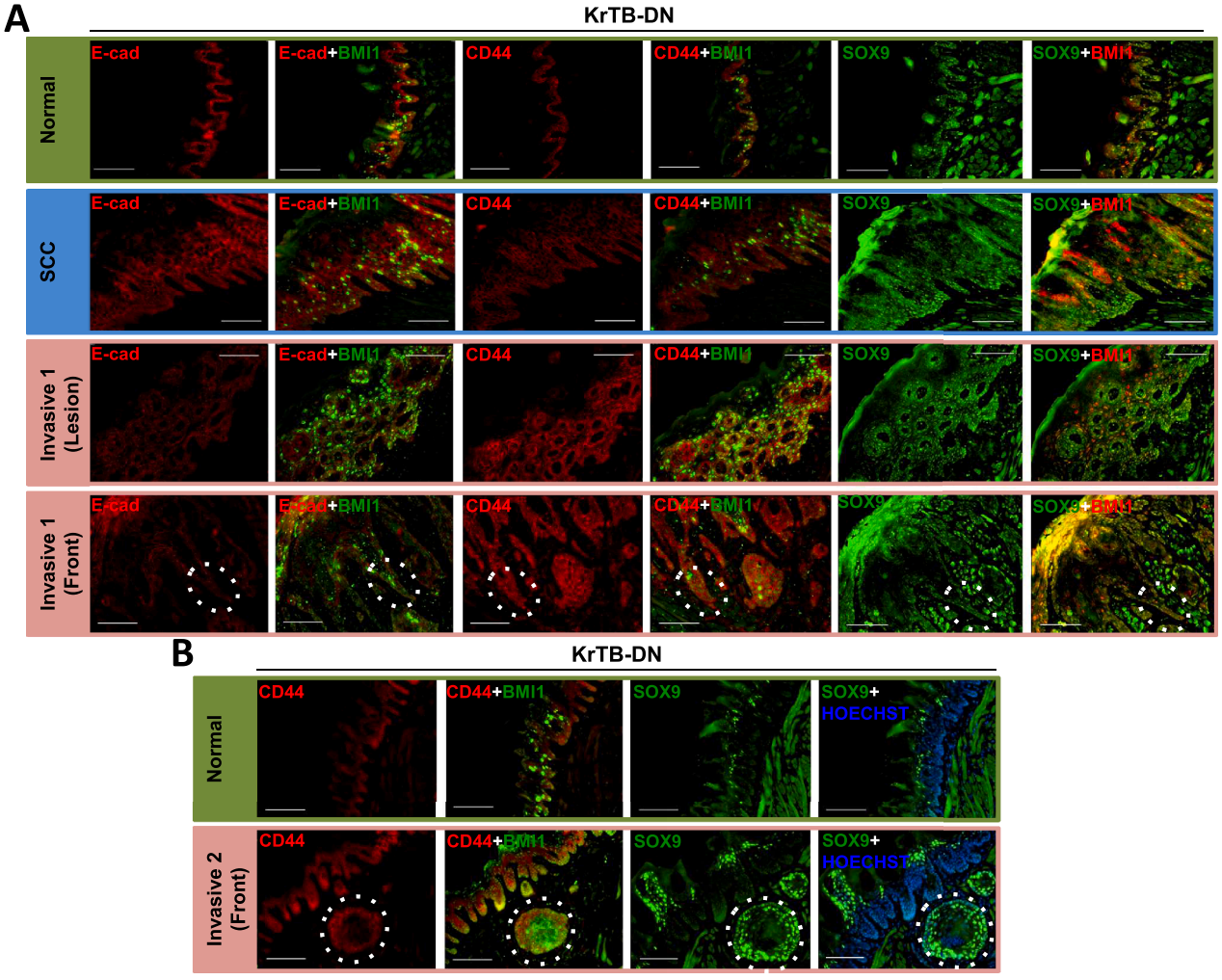

Fig. 4. BMI1 and SOX9 are detected in the infiltrating cells of invasion fronts. (**A**) BMI1, E-cadherin, CD44, and SOX9 IF stainings in normal, in-situ SCC, invasive lesion, and invasive front samples from KrTB-DN tongues. Two KrTB-DN tongues exhibited invasive SCCs. Representative fields are shown. Same lesion area is circled in "Invasive 1 (Front)" panels for comparison (200X; scale bar: 100 μm). (**B**) BMI1, CD44, and SOX9 IF signals in normal and invasive front samples from a second KrTB-DN tongue. Representative fields are shown. Same lesion area is circled in "Invasive 2 (Front)" panels for comparison (200X; scale bar: 100 μm). For **A-B**, two different SOX9 antibodies were used for further validation.

also exhibited cells with high BMI1, CD44, and SOX9 expression infiltrating adjacent tongue muscle (circled areas, Fig. 4B).

We also examined GLUT1 (SLC2A1) in invasive tongue lesions, as the SLC2A1 transcript is associated with OSCC and SLC2A1 was further increased in KrTB-DN compared to KrTB-N tongues (see Fig. 2D). GLUT1 protein was expressed in basal SCs of normal oral epithelia in KrTB-DN (Fig. 5A) and KrTB-N (Fig. 5B), as well as in *in-situ* SCC lesions of KrTB-N mice (Fig. 5B). Importantly, GLUT1 protein levels in SCC lesions of both KrTB-DN (Fig. 5A) and KrTB-N (Fig. 5B) were greater than their counterpart normal oral epithelia. The invasive lesions and the infiltrating cells in underlying muscle tissue in a KrTB-DN tongue were positive for BMI1 and GLUT1 and expressed decreased levels of E-cadherin (see circled areas, Fig. 5A). Collectively, our IF data show that BMI1, SOX9, and GLUT1 are detected at OSCC invasion fronts.

Metabolomic data show that BMI1 overexpression in tongue epithelia promotes glycolysis during 4-NQO-induced carcinogenesis

We identified infiltrating cells in invasion fronts with high levels of the OSCC-associated factor GLUT1, and this glycolysis marker is involved in glucose uptake in mammalian cells [28]. Furthermore, our RNA-seq data revealed that other glycolysis markers, as well as two transcripts which encode citrate cycle enzymes, were increased in KrTB-DN compared to KrTB-N tongues (Sup. Fig. 6). Thus, we evaluated the effects of BMI1 overexpression on levels of different metabolites from tongue epithelia. We identified the pathways that are over-represented by assessing significant changes in levels of measured metabolites from KrTB-D vs. KrTB, and KrTB-DN vs. KrTB-N tongues. While "Phenylalanine, tyrosine, and tryptophan biosynthesis" and "Pentose phosphate pathway" were among the most significantly altered pathways in KrTB-D vs. KrTB mice (Sup. Fig. 7A), "Citrate cycle (TCA cycle)" and "Glycolysis or Gluconeogenesis" were among the most significantly

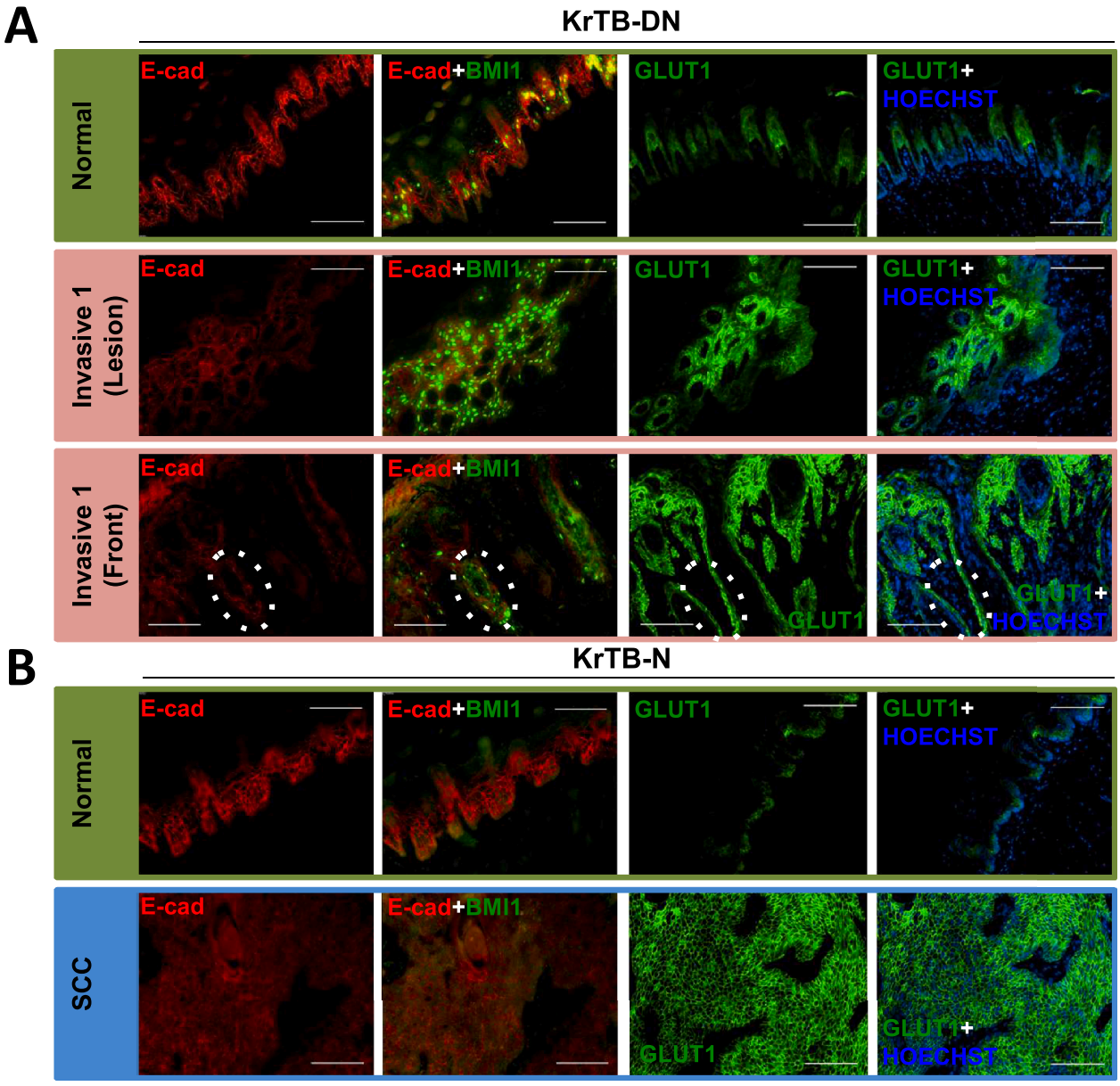

Fig. 5. GLUT1 is also detected in the infiltrating cells of invasion fronts. (**A**) BMI1, E-cadherin, and GLUT1 stainings in normal, invasive lesion, and invasive front samples from KrTB-DN tongues. Two KrTB-DN tongues exhibited invasive SCCs. Same lesion area is circled in "Invasive 1 (Front)" panels for comparison. (**B**) BMI1, E-cadherin, and GLUT1 stainings in normal and in-situ SCC samples from KrTB-N tongues. Only one KrTB-N tongue exhibited in-situ SCCs. For **A-B**, representative fields are shown (200X; scale bar: 100 μm).

altered in KrTB-DN vs. KrTB-N tongues (Sup. Fig. 7B).

The levels of 15 metabolites involved in glycolysis/gluconeogenesis were not changed in normal tongue epithelia by BMI1 overexpression (compare KrTB-D vs. KrTB for each metabolite in Fig. 6). However, 14 of these 15 metabolites were increased in KrTB-DN compared to KrTB-N tongue epithelia (Fig. 6A-D, 6F-O), with the exception of Fructose 6-Phosphate, which was decreased (Fig. 6E). While metabolites resulting from the first steps in the TCA cycle were decreased (Sup. Fig. 8A-B), metabolites produced by later TCA cycle reactions were significantly increased in KrTB-DN vs. KrTB-N tongues (Sup. Fig. 8C-G). Finally, some metabolites involved in the Pentose phosphate pathway and Purine metabolism were also increased in KrTB-DN compared to KrTB-N tongues (Sup. Fig. 8H-N).

Overall, these results indicate that BMI1 overexpression in tongue epithelia influences energy generation, promoting glycolysis. Survival analysis of human head and neck cancer samples from the Human Protein Atlas show that high SOX9 expression correlate with lower survival probability (P score = 0.008, Sup. Fig. 9A) [37]. Furthermore, genome-wide ChIP sequencing data compiled by the UCSC Genome Browser show that SOX9 associates with the promoters of glycolytic genes SLC2A1 and PKM in other cell types (Sup. Fig. 10). As BMI1 associates with the promoter region of the SOX9 gene in our KrTB model (Sup. Fig. 3), these results suggest that downstream target SOX9 is involved in the glycolytic changes observed upon BMI1 overexpression during 4-NQO-induced carcinogenesis.

Discussion

When ectopic BMI1 is overexpressed, HIF1α and SOX9 are further increased by 4-NQO

We previously reported that high, exogenous BMI1 expression in basal SCs enhanced tumor formation upon carcinogen treatment in the HNSCC model [20]. Here, we delineate the molecular features that lead to more severe tumors upon high BMI1 expression. For instance, our data show that SOX9 and HIF1α mRNAs (Fig. 2C) and proteins (Fig. 3) are further increased in 4-NQO-treated tongue epithelia when BMI1 is overexpressed.

SOX9 has been identified as a poor prognostic factor for OSCC. SOX9 expression is increased in *in vitro* HNSCC models such as in R-HSC-3 cells where SOX9 was linked to multidrug resistance [38], and in CAL27 cells where SOX9 promoted stemness and epithelial-mesenchymal transition (EMT) [39]. Cytoplasmic SOX9 expression was reported in OSCC cells of surgical specimens from patients, and this cytoplasmic pattern was positively correlated with poor clinical outcomes [33]. Other studies further confirmed that high SOX9 expression patterns in patients with OSCC result in enhanced tumor radioresistance [40] and worse overall survival [26]. Furthermore, survival analysis of human head and neck cancer samples from the Human Protein Atlas show that high SOX9 expression correlate with lower survival probability (P score = 0.008, Sup. Fig. 9A) [37]. Our data in KrTB mice showed that SOX9 levels followed a similar trend compared to BMI1 expression and were

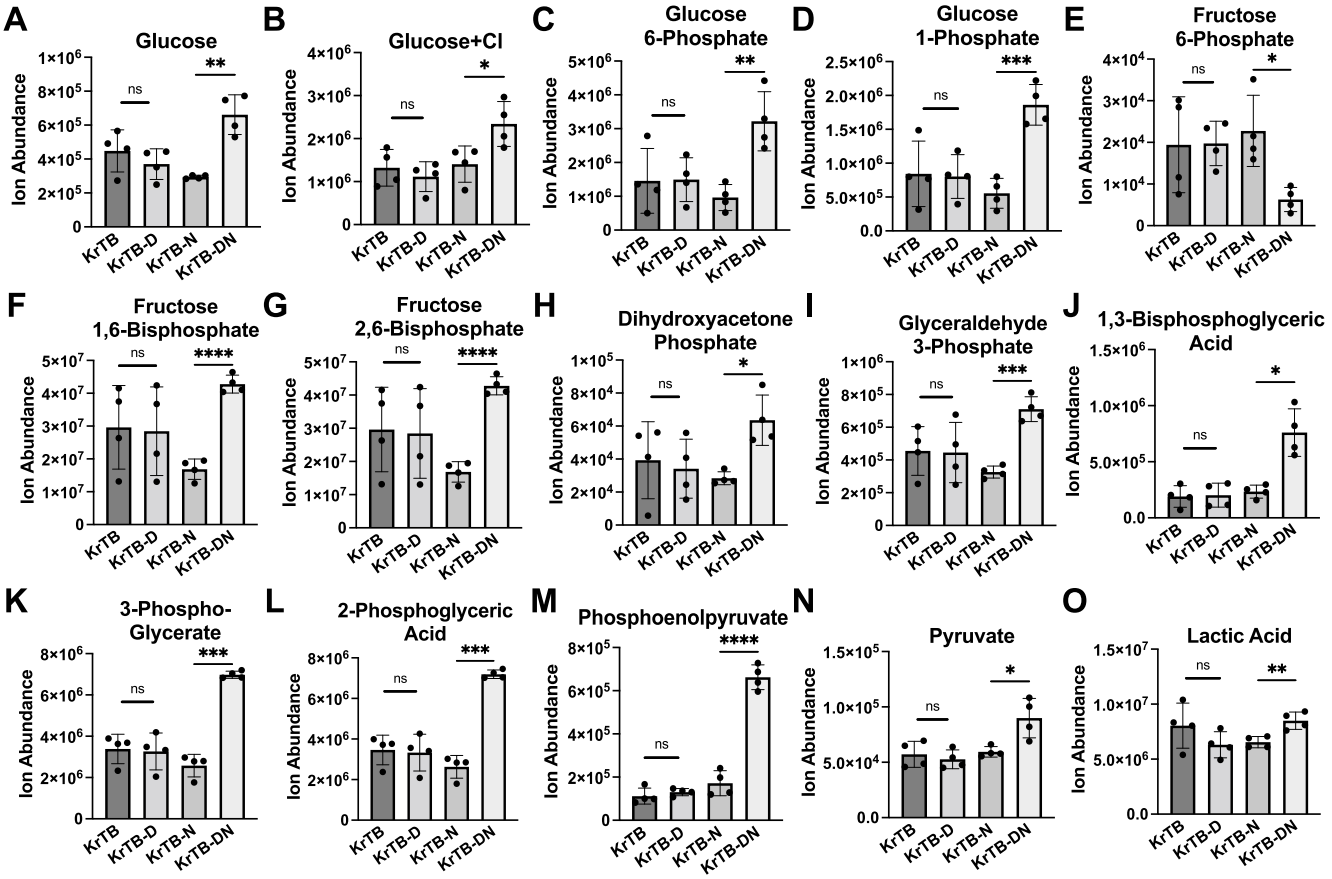

Fig. 6. BMI1 overexpression in tongue epithelia promotes glycolysis during 4-NQO-induced carcinogenesis. Levels of (**A**) Glucose, (**B**) Glucose+Cl, (**C**) Glucose 6-Phosphate, (**D**) Glucose 1-Phosphate, (**E**) Fructose 6-Phosphate, (**F**) Fructose 1,6-bisphosphate, (**G**) Fructose 2,6-bisphosphate, (**H**) Dihydroxyacetone Phosphate, (**I**) Glyceraldehyde 3-Phosphate, (**J**) 1,3-Bisphosphoglyceric Acid, (**K**) 3-Phosphoglycerate, (**L**) 2-Phosphoglyceric Acid, (**M**) Phosphoenolpyruvate, (**N**) Pyruvate, and (**O**) Lactic Acid in KrTB, KrTB-D, KrTB-N, and KrTB-DN tongue epithelia (N = 4/group). Data graphed denotes the mean of Ion Abundance ± standard deviation of the mean (SD). Statistical significance was determined using Welch's t-test for KrTB-D vs. KrTB, and for KrTB-DN vs. KrTB-N. *0.01<p<0.05, **0.001<p<0.01, ***0.0001<p<0.001, ****p<0.0001.

increased by both DOX and 4-NQO (Figs. 2C and 3B). As we detected SOX9 together with BMI1 in the infiltrating cells of invasion fronts (Fig. 4), we propose that the suggested transcriptional activation of SOX9 by BMI1 (Sup. Fig. 3) is in part responsible for the increase in the severity of tongue tumors in KrTB-DN compared to KrTB-N mice (Fig. 1F).

Multiple reports have linked HIF1α to human OSCC. HIF1α is a transcriptional activator for multiple genes that contain hypoxia-responsive elements (HREs) [41] and are involved in processes such as metabolism, proliferation, invasion, and metastasis [42]. HIF1α is detected in nuclear and cytoplasmic regions of neoplastic cells from OSCC patients [43]. While HIF1α expression patterns in OSCC patients are different depending on tumor location and subtype, over 90 % of metastatic lymph nodes analyzed showed HIF1α-positive tumor cells [44]. HIF1α is also a key promoter of energy adaptation based on the availability of nutrients and oxygen in distinct OSCC tumor microenvironments [45]. Furthermore, when HIF1α expression was suppressed in the human SCC-15 cell line under normoxic or hypoxic conditions, cell growth and invasion were inhibited [46].

Although these reports indicate that HIF1α is a key factor involved in energy metabolism and invasion potential of OSCC cells, survival analysis of human head and neck cancer samples from the Human Protein Atlas show that low HIF1A expression does not necessarily correlate with higher survival probability (P score = 0.19, Sup. Fig. 9B) [37]. Also, while we previously demonstrated that ectopic BMI1 overexpression for two weeks increases HIF1α protein expression and drives hypoxic signaling, including metabolic reprograming, in *normal* oral cavity epithelia [21], here we report that this increase in HIF1α is not observed after 25 weeks of continuous dox treatment (KrTB-D vs. KrTB, Fig. 3C). In contrast, HIF1α protein expression was *only* increased upon ectopic BMI1 overexpression for 25 weeks when mice were also given 4-NQO (KrTB-DN vs. KrTB-N, Fig. 3C). Thus, our results indicate specific effects of BMI1 overexpression on various proteins in tongue epithelia over time. More studies are needed to fully characterize the complex spatiotemporal associations between BMI1 and HIF1α, as well as their potential effects on OSCC onset and/or development.

Other transcripts associated with OSCC are increased by 4-NQO when ectopic BMI1 is overexpressed

Examples of other targets that are increased in KrTB-DN vs. KrTB-N tongues. (Fig. 2C) include transcripts encoding S100 proteins S100A8 and S100A9, which are involved in the initiation and progression of HNSCC via multiple signaling pathways [47]. Lipocalin-2 (LCN2) mRNA is also increased in KrTB-DN vs. KrTB-N tongues. (Fig. 2C). Lipocalin-2 (LCN2) is part of the innate immune response to bacterial infections; however LCN2 mRNA is upregulated during OSCC metastasis and LCN2 protein directly binds to EGFR to induce cell proliferation and downstream signal activation [48]. The mRNA levels of multiple matrix metalloproteinases (MMPs) that play important roles in tumor invasion and metastasis, including MMP9, are increased in KrTB-DN vs. KrTB-N tongues (Fig. 2C) and in human HNSCC samples [49].

Additional transcripts increased in KrTB-DN vs. KrTB-N tongues include IL1B, ALDH1A3, and PD-L1 (Fig. 2C). IL1B, an inflammatory cytokine involved in EMT regulation, cancer development, and distant metastasis, also promotes drug resistance in a HNSCC mouse model [50]. Aldehyde dehydrogenase 1 family member A3 (ALDH1A3), which is involved in alcohol metabolism and oxidative stress and which we previously identified as a potential biomarker for HNSCC [51], is increased in advanced stage human HNSCCs compared to normal tissue [52]. mRNA Levels of programmed death ligand 1, PD-L1 (CD274 gene) are increased in KrTB-DN vs. KrTB-N tongues (Fig. 2C). PD-L1 is elevated in HNSCC patients and is associated with resistance to cancer therapies. PD-L1 mRNA is significantly decreased by nimotuzumab and this results in increased tumor sensitivity for further chemotherapeutic treatments [53]. We propose that elevated levels of these and other OSCC associated transcripts in tongue epithelia (Fig. 2C) account for the increased severity of tongue tumors in KrTB-DN compared to KrTB-N mice (Fig. 1F).

Other transcripts increased in KrTB-DN vs. KrTB-N tongues include SOX9 putative targets (Fig. 2D). Glucose transporter 1 (GLUT1/SLC2A1) is a key enzyme that regulates the rate of glycolysis, as it facilitates the uptake of glucose across plasma membranes of mammalian cells [28]. Interestingly, the SLC2A1 gene contains HRE sites and thus its expression is likely regulated by HIF1α [54], which is also increased in KrTB-DN vs. KrTB-N tongues (Fig. 3C). High GLUT1 levels in samples correlate with lymph node metastasis [55] and with poorer overall survival of HNSCC patients [28]. More specifically, GLUT1 overexpression has been linked with tumor size and regional invasiveness [56]. Here, we showed that GLUT1, together with BMI1, are detected in the infiltrating cells of invasion fronts (Fig. 5), in agreement with these reports.

Additional SOX9 putative targets increased in KrTB-DN vs KrTB-N tongues include transcripts for INHBB, MYOF, EPHA2, and TNC (Fig. 2D). Inhibin beta B (INHBB) is the subunit of the homodimer Activin B with roles in processes such as inflammation, proliferation, and immune regulation [29]. INHBB-positive cells are increased in OSCC compared to normal samples [29] and significantly correlate with EMT and regional lymph node metastasis [57]. Myoferlin (MYOF), a factor first characterized in muscle cells and involved in calcium-mediated membrane fusion events and vesicle trafficking, is correlated with poor patient survival in oropharyngeal SCC [30]. Ephrin receptor A2 (EPHA2) is a type of tyrosine kinase receptor that enhances proliferation, stemness, invasion, and metastasis in cancer by promoting the nuclear translocation of YAP, an effector of the Hippo pathway [31]. Finally, increased Tenascin-C (TNC) levels, a protein expressed in the extracellular matrix and involved in inflammation responses, are detected in invasive lesions and correlated with shorter survival times in patients [32]. Increases in these target transcripts in samples from KrTB-DN vs. KrTB-N mice suggest how 4-NQO-induced tongue tumors could become more invasive when ectopic BMI1 is overexpressed.

Ectopic BMI1 expression during OSCC increases pathways linked to metabolic reprogramming

BMI1 is increased in cancer stem cells (CSCs) [19], and these cells can initiate and maintain oral tumors [58]. Cancer cells can adapt to more glycolytic pathways to generate their energy, instead of oxidative phosphorylation, in what is known as the Warburg effect [41,59]. Metabolic reprograming, specifically increased glucose metabolism, is a key feature in HNSCC and provides the energy to support rapid and uncontrolled cell proliferation, as well as tumor progression [59]. Notably, when BMI1 is inhibited in a HNSCC xenograft model, cell proliferation is reduced [60], and our data show that epithelial SCs proliferate faster in 4-NQO-induced tongues upon BMI1 overexpression (Sup. Fig. 4), in agreement with these findings.

Furthermore, multiple glycolytic genes, including GLUT1, HK2, and PKM, are activated in tumor cells [59,61]. Cancer cells metabolize most glucose available to lactate, despite the availability of oxygen, and promote the use of resulting glycolytic metabolites in anabolic processes such as in the synthesis of ribonucleotides, key building blocks in DNA and RNA molecules [59]. We previously performed real-time cell metabolic assays to show that BMI1 overexpression, as reported in OSCCs, was sufficient to decrease oxidative phosphorylation and increase glycolysis in the human oral cell line OKF6-TERT1R [21]. Here, our RNA-seq analyses show that carboxylic acid transport, HIF-1 signaling, and central carbon metabolism in cancer are among the top upregulated processes and pathways with ectopic BMI1 overexpression in 4-NQO-treated tongues (Sup. Fig. 1C-D). We identified mRNAs for multiple glycolytic markers, including GLUT1, HK2, and PKM, that were increased in KrTB-DN compared to KrTB-N tongues (Fig. 2D and Sup. Fig. 6). Finally, our metabolomics data collected from tongue epithelia

show that BMI1 overexpression during 4-NQO treatment also increased the levels of metabolites resulting from glycolysis and from anabolic processes such as the pentose phosphate pathway and purine metabolism (Fig. 6 and Sup. Fig. 8). Thus, our results demonstrate that ectopic BMI1 further induces metabolic pathways involved in metabolic reprograming during oral carcinogenesis.

Additional studies are necessary to fully delineate how BMI1 further promotes glycolysis during 4-NQO treatment. We demonstrated that BMI1 associates with the HIF1A promoter region in tongue epithelia of KrTB mice [21]. HIF1α is a key factor involved in metabolic reprograming, as it associates with and increases the expression of several genes that encode for glycolytic enzymes, such as HK2, GLUT1, LDHA, and PKM [54,59]. Here, we report that BMI1 associates with the SOX9 promoter region as well (Sup. Fig. 3). Interestingly, SOX9 protein can directly bind to the HK2 promoter, and thus stimulates glycolysis in colon cancer cells [62]. Furthermore, genome-wide ChIP sequencing data compiled by the UCSC Genome Browser show that SOX9 associates with the promoters of SLC2A1 and PKM in other cell types (Sup. Fig. 10), including chondrocytes, fetal Sertoli, and skin cells, as well as with the promoters of all of the metabolic targets shown in Sup. Fig. 6 in these types of cells [27,63,64]. Thus, in future studies we want to determine if BMI1 can directly bind to glycolytic genes in tongue epithelia during 4-NQO-induced tumorigenesis or if these increases occur through the actions of BMI1 downstream targets SOX9 and/or HIF1A.

Conclusions

We conclude that high BMI1 expression aggravates 4-NQO-induced tumorigenesis by increasing the expression of transcripts and proteins of OSCC promoting factors, such as SOX9, HIF1A, GLUT1, MMP9, INHBB, and MYOF, as well as metabolic enzymes such as LDHA, PGK1, PKM, PFKL, and HK2. As many of these factors are linked to the metabolic reprograming that occurs during carcinogenesis, BMI1 influences how OSCC cells generate energy by glycolysis.

Materials and methods

K14-rtTA;TRE-FLBmi-1 mice and doxycycline treatment

K14-rtTA;TRE-FLBmi-1 mice (abbreviated as KrTB, RRID: MGI_7840083) were generated, described, and characterized before [20, 21]. At 6 weeks of age, female KrTB mice were treated with 2 mg/ml doxycycline hyclate (Sigma; D9891-25G) added to the drinking water [20], and replenished twice a week (KrTB-D mice). Doxycycline (DOX) treatment continued for 25 weeks, after which the mice were sacrificed. We gave DOX-containing water to adult mice (starting at 6 weeks of age) to avoid any possible developmental effects of Bmi1 overexpression. Before all mice were sacrificed, regular and DOX-containing water bottles were removed from cages for 1.5 h and placed back for an additional 1.5 h. The mouse line, treatments, and abbreviations used are indicated (Fig. 1B).

4-nitroquinoline 1-oxide (4-NQO) administration and tissue dissection

Cohorts of female KrTB mice treated with DOX for 25 weeks and age-matched, "No-DOX" KrTB mice were also treated with 50 μg/ml 4-NQO (Sigma Aldrich; D9891) in the drinking water for the first 10 weeks (KrTB-DN and KrTB-N groups, respectively, $N = 9$-13 per group, Fig. 1B) as previously described [17,18,20,22,65]. Mouse tongues were isolated 15 weeks after the termination of the 10-week 4-NQO treatment. For this study, we used a lower concentration of 4-NQO in the drinking water (50 μg/ml) to delineate possible effects of ectopic BMI1 on tumorigenesis, as the 4-NQO dose previously used (100 μg/ml in the drinking water) resulted in tumorigenic lesions in all groups of treated mice [20,22,25]. Age-matched, KrTB (no DOX) and KrTB-D (DOX-treated) mice were also included as controls (N = 5-10 per group, Fig. 1B). All tongues were dissected and photographed immediately after cervical dislocation.

Histological analysis of tongue lesions

Neoplastic lesions on all tongues were imaged and identified. We counted all visible lesions on each tongue [20,22,66] in a blinded manner (X.T.). For pathological classification, a portion of tongue tissue was fixed in 4 % paraformaldehyde (PFA; Sigma; #P6148) overnight. Tissues were processed and sectioned at 5–7 μm in the Weill Cornell Electron Microscopy and Histology Core. The histological diagnosis of squamous neoplasia was performed by a board-certified head and neck pathologist (T.S.) on hematoxylin and eosin (H&E)-stained tissue samples in a blinded manner [17,18,20,22,65]. The most severe lesion in each mouse was categorized as: hyperplasia, dysplasia (including mild, moderate, and severe), in-situ squamous cell carcinoma (in-situ SCC), or invasive SCC [17,20,22].

Immunohistochemistry (IHC) and immunofluorescence (IF)

Tissues for IHC and IF were harvested immediately after cervical dislocation, fixed in 4 % paraformaldehyde overnight, and subsequently processed and sectioned. We performed IHC staining as described [66, 67]. For IF staining, we performed deparaffinization, rehydration, antigen retrieval on paraffin-embedded sections, blocking, primary/secondary antibody incubations, Sudan Black B quenching, and mounting as previously described [22]. The antibodies and conditions used in IHC and IF are shown (Supplementary Table 3). All images were acquired on a Nikon Eclipse TE2000-E microscope using NIS-Elements AR software. 200X magnification was used for all IHC and IF images.

Quantification of immunostaining

To quantify the intensity of staining, the signals for IHC were analyzed using the Fiji (ImageJ) software (National Institutes of Health, RRID:SCR_003070), and values were normalized as indicated in figures and as previously described [22]. For consistency among all groups, we quantified expression levels in normal epithelia of KrTB-N (N, 4-NQO) and KrTB-DN (DN, DOX+4-NQO) mice, as groups not treated with 4-NQO did not exhibit visible pre-neoplastic/neoplastic tongue lesions. All IHC quantifications were performed using 4-5 representative fields per section (as shown in each figure), with slides from $N = 3$ mice per experimental condition analyzed. For IF, we stained the most severe lesions from each 4-NQO-treated group.

RNA isolation, genome-wide RNA sequencing (RNA-seq), and data analysis

Total RNA was isolated from ~3 mg of tongue epithelia collected from at least four female mice/group (25-week time points, Fig. 1B). At 6 weeks of age, these mice were treated with or without DOX and/or 4-NQO as described above, and all tongues were collected from mice that were 31 weeks old. Epithelia were separated from the rest of the tongues, saved in RNALater, and homogenized as described [21]. The RNeasy Micro Kit (Qiagen; 74004) was used for RNA isolation, following the manufacturer's protocol. Final products were eluted from columns using 14 μl of UltraPure distilled water [21]. RNA integrity number (RIN) measurements, cDNA library preparation, and deep sequencing were carried out by the Genomics Resources Core Facility of WCMC, as described [68]. Differential expression analyses were performed using DESeq2 v1.6.3 (RRID:SCR_000154) as before [68]. Volcano plots and pathway enrichment analyses were completed using BioJupies (RRID: SCR_016346, https://maayanlab.cloud/biojupies), a web server application designed by the Ma'ayan Lab at the Icahn School of Medicine (Mount Sinai) [69]. The RNA-seq data has been deposited in GEO (NCBI) repository (accession number GSE285101) and is embargoed until publication.

qPCR using DNA fragments eluted after chromatin immunoprecipitation (ChIP) assay

Chromatin immunoprecipitation (ChIP) was performed using a BMI1 antibody (Cell Signaling Cat# 6964S, RRID: AB_10828713) and tongue epithelia from KrTB mice treated with doxycycline for 2 weeks and age-matched, untreated KrTB mice [21]. Resulting DNA fragments were eluted from BMI1-bound immunocomplexes, purified, and assayed for SOX9 by qPCR ($N = 3$ per experimental group). The SOX9 primers are: SOX9 Promoter (F) 5′- AAAATCCGGTCCAATCAGCG-3′ and SOX9 Promoter (R) 5′- TTCACGTTAGATACCTCGGGC-3′. These primers were designed to amplify a region in the SOX9 promoter that is bound by other transcription factors, as shown by ChIP-seq data compiled by the UCSC Genome Browser (RRID:SCR_005780, Sup. Fig. 4A). 1 µl of eluted, purified DNA and 1 µl of 1:100 diluted input DNA were used as templates for the qPCR reactions.

We also isolated the DNA fragments that were immunoprecipitated by the BMI1 antibody and amplified using the SOX9 primers (Sup. Fig. 4B). Sanger sequencing (GENEWIZ) confirmed that these fragments matched a region in the SOX9 Promoter (Sup. Fig. 4C).

Untargeted metabolomics

We extracted metabolites from snap-frozen tongue epithelium samples and subjected them to untargeted metabolomics using an LC system as described [68]. Metabolites were extracted from ~3 mg of tongue epithelia collected from four female KrTB mice/group (groups in Fig. 1B). For normalization purposes, pellets were solubilized as described, and amounts of protein relative to bovine serum albumin standards (0-1.5 mg/ml) were determined using the BioRad assay [68]. Raw data files were processed as before, using MassHunter Qualitative Analysis Software (B07.00; Agilent Technologies), with downstream comparative data analysis performed using MassHunter Profinder (B08.00) and MassProfiler Professional (Agilent, B14.5) [68]. Data will be available upon request.

Statistics

Statistical analysis was performed on at least 3 samples from each group using GraphPad Prism 8 (RRID:SCR_002798). Data are represented as mean ± SD and normalized as indicated in the figure legends. RNA-seq analyses include at least 4 independent biological replicates/group. qPCR after ChIP includes 3 independent biological replicates/group. p-Values for all protein expression signals from IHC were determined using one-way ANOVA followed by Turkey's test. p-Values for amounts of DNA IPed (ChIP on mouse epithelia) were determined using Welch's t-test. p-Values for amounts of each metabolite in tongue epithelia (metabolomics) were also determined using Welch's t-test. Significance of the distribution of lesion numbers and lesion pathology among the groups was analyzed using chi-square test. A p value of <0.05 was considered as statistically significant. p-Values are indicated as *$0.01<p<0.05$, **$0.001<p<0.01$, ***$0.0001<p<0.001$, ****$p<0.0001$.

Ethical statement

The care and use of animals in this study were approved by the Institutional Animal Care and Use Committee (IACUC) of Weill Cornell Medical College, and conformed to the US National Institutes of Health guidelines for the humane care and use of laboratory animals.

Data and materials availability

The RNA-seq data have been deposited in the GEO (NCBI) repository (accession number GSE285101) and is embargoed until publication. The metabolomic data will be available upon request. All other data needed to evaluate the conclusions in the paper are available in the main text or the supplementary materials.

Funding

This research was supported by National Institutes of Health (T32 CA062948 to J.B. and RO1 CA205258 to L.J.G.), and Weill Cornell Medicine Funds (*JumpStart* Career Development Award to J.B.).

CRediT authorship contribution statement

Jorge Baquero: Writing – original draft, Visualization, Methodology, Investigation, Funding acquisition, Formal analysis, Conceptualization. **Xiao-Han Tang:** Writing – review & editing, Methodology, Formal analysis, Data curation, Conceptualization. **Daniel Galke:** Investigation, Formal analysis. **Theresa Scognamiglio:** Formal analysis, Data curation. **Tuo Zhang:** Formal analysis, Data curation. **Dawson Miller:** Methodology, Formal analysis. **Qiuying Chen:** Methodology, Formal analysis. **Steven Gross:** Methodology, Formal analysis. **Lorraine J. Gudas:** Writing – review & editing, Supervision, Project administration, Methodology, Funding acquisition, Conceptualization.

Declaration of competing interest

The authors declare that they have no known competing financial interests or personal relationships that could have appeared to influence the work reported in this paper.

Acknowledgments

The authors sincerely thank Dr. Marta Melis, Dr. Krysta Dikun, and other Gudas lab colleagues for their outstanding technical assistance and scientific contributions, which propelled this research forward. Furthermore, we would like to thank the EM Core Facility at Weill Cornell Medical College for their exceptional work on slide preparation, and the Weill Cornell Genomics Resources Core Facility for guidance on RNA sequencing.

Supplementary materials

Supplementary material associated with this article can be found, in the online version, at doi:10.1016/j.neo.2025.101146.

References

[1] R.L. Siegel, K.D. Miller, N.S. Wagle, A. Jemal, Cancer statistics, 2023, CA Cancer J. Clin. 73 (1) (2023) 17–48.
[2] R.L. Siegel, A.N. Giaquinto, A. Jemal, Cancer statistics, 2024, CA Cancer J. Clin. 74 (1) (2024) 12–49.
[3] D.E. Johnson, et al., Head and neck squamous cell carcinoma, Nat. Rev. Dis. Prim. 6 (1) (2020) 92.
[4] A. Chamoli, et al., Overview of oral cavity squamous cell carcinoma: risk factors, mechanisms, and diagnostics, Oral Oncol. 121 (2021) 105451.
[5] A. Bhatia, B. Burtness, Treating head and neck cancer in the age of immunotherapy: a 2023 update, Drugs 83 (3) (2023) 217–248.
[6] Q. Hu, et al., The poor outcome of second primary oral squamous cell carcinoma is attributed to BMI1 upregulation, Cancer Med. 4 (2018) 1056–1069.
[7] T. Tanaka, et al., BMI1-positive cells in the lingual epithelium could serve as cancer stem cells in tongue cancer, Sci. Rep. 6 (2016) 39386.
[8] R.S. Rao, K.L. Raju, D. Augustine, S. Patil, Prognostic significance of ALDH1, BMI1, and OCT4 expression in oral epithelial dysplasia and oral squamous cell carcinoma, Cancer Control J. Moffitt Cancer Cent. 27 (1) (2020) 1073274820904959.
[9] L. Di Croce, K. Helin, Transcriptional regulation by polycomb group proteins, Nat. Struct. Mol. Biol. 20 (10) (2013) 1147–1155.
[10] M. Sauvageau, G. Sauvageau, Polycomb group proteins: multi-faceted regulators of somatic stem cells and cancer, Cell Stem Cell 7 (3) (2010) 299–313.
[11] J.H. Vissers, M. van Lohuizen, E. Citterio, The emerging role of polycomb repressors in the response to DNA damage, J. Cell Sci. 125 (Pt 17) (2012) 3939–3948.
[12] H. Wang, et al., Role of histone H2A ubiquitination in polycomb silencing, Nature 431 (7010) (2004) 873–878.

[13] S. Zhu, et al., BMI1 regulates androgen receptor in prostate cancer independently of the polycomb repressive complex 1, Nat. Commun. 9 (1) (2018) 500.
[14] S. Banerjee Mustafi, et al., Mitochondrial BMI1 maintains bioenergetic homeostasis in cells, FASEB J. 30 (12) (2016) 4042–4055. *: official publication of the Federation of American Societies for Experimental Biology*.
[15] K.B. Jones, et al., Quantitative clonal analysis and single-cell transcriptomics reveal division kinetics, hierarchy, and fate of oral epithelial progenitor cells, Cell Stem Cell 24 (1) (2019) 183–192, e188.
[16] T. Okubo, C. Clark, B.L. Hogan, Cell lineage mapping of taste bud cells and keratinocytes in the mouse tongue and soft palate, Stem Cells (1981) 27 (2) (2009) 442–450.
[17] X.H. Tang, B. Knudsen, D. Bemis, S. Tickoo, L.J. Gudas, Oral cavity and esophageal carcinogenesis modeled in carcinogen-treated mice, Clinic. Cancer Res. 10 (1 Pt 1) (2004) 301–313. *: an official journal of the American Association for Cancer Research*.
[18] X.H. Tang, T. Scognamiglio, L.J. Gudas, Basal stem cells contribute to squamous cell carcinomas in the oral cavity, Carcinogenesis 34 (5) (2013) 1158–1164.
[19] D. Chen, et al., Targeting BMI1(+) cancer stem cells overcomes chemoresistance and inhibits metastases in squamous cell carcinoma, Cell Stem Cell 20 (5) (2017) 621–634, e626.
[20] J.M. Kalish, X.H. Tang, T. Scognamiglio, T. Zhang, L.J. Gudas, Doxycycline-induced exogenous BMI-1 expression enhances tumor formation in a murine model of oral squamous cell carcinoma, Cancer Biol. Ther. 21 (5) (2020) 400–411.
[21] J. Baquero, et al., The transcription factor BMI1 increases hypoxic signaling in oral cavity epithelia, Biochim. Biophys. Acta Mol. Basis. Dis. 1870 (5) (2024) 167161.
[22] J. Baquero, X.H. Tang, T. Scognamiglio, L.J. Gudas, EZH2 knockout in oral cavity basal epithelia causes more invasive squamous cell carcinomas, Carcinogenesis 42 (12) (2021) 1485–1495.
[23] M. Melis, T. Zhang, T. Scognamiglio, L.J. Gudas, Mutations in long-lived epithelial stem cells and their clonal progeny in pre-malignant lesions and in oral squamous cell carcinoma, Carcinogenesis 41 (11) (2020) 1553–1564.
[24] I. Sequeira, et al., Genomic landscape and clonal architecture of mouse oral squamous cell carcinomas dictate tumour ecology, Nat. Commun. 11 (1) (2020) 5671.
[25] X.H. Tang, et al., Gene expression profiling signatures for the diagnosis and prevention of oral cavity carcinogenesis-genome-wide analysis using RNA-seq technology, Oncotarget 6 (27) (2015) 24424–24435.
[26] S. Steen, et al., Expression analysis of SOX_2 and SOX_9 in patients with oral squamous cell carcinoma, Head Neck 47 (2) (2025) 437–451.
[27] M. Kadaja, et al., SOX9: a stem cell transcriptional regulator of secreted niche signaling factors, Genes Dev. 28 (4) (2014) 328–341.
[28] Y. Wang, et al., Prognostic value of glycolysis markers in head and neck squamous cell carcinoma: a meta-analysis, Aging 13 (5) (2021) 7284–7299.
[29] Y.Y. Chung, S.J. Cheng, H.H. Ko, W.Y. Shie, H.Y. Elizabeth Chou, Evaluation of the prognostic and therapeutic potential of inhibin beta B for oral squamous cell carcinoma, J. Dent. Sci. 19 (1) (2024) 448–454.
[30] B. Kumar, et al., High expression of myoferlin is associated with poor outcome in oropharyngeal squamous cell carcinoma patients and is inversely associated with HPV-status, Oncotarget 7 (14) (2016) 18665–18677.
[31] J. Bai, et al., EphA2 promotes the transcription of KLF4 to facilitate stemness in oral squamous cell carcinoma, Cell. Mol. Life Sci. CMLS 81 (1) (2024) 278.
[32] C. Spenlé, et al., Tenascin-C orchestrates an immune-suppressive tumor microenvironment in oral squamous cell carcinoma, Cancer Immunol. Res. 8 (9) (2020) 1122–1138.
[33] Y. Sumita, et al., Cytoplasmic expression of SOX9 as a poor prognostic factor for oral squamous cell carcinoma, Oncol. Rep. 40 (5) (2018) 2487–2496.
[34] J. Zhou, et al., Clinical and prognostic significance of HIF-1α overexpression in oral squamous cell carcinoma: a meta-analysis, World J. Surg. Oncol. 15 (1) (2017) 104.
[35] Z. Abdalla, T. Walsh, N. Thakker, C.M. Ward, Loss of epithelial markers is an early event in oral dysplasia and is observed within the safety margin of dysplastic and T1 OSCC biopsies, PLoS One 12 (12) (2017) e0187449.
[36] D.&. Chen, C.Y. Wang, Targeting cancer stem cells in squamous cell carcinoma, Precis. Clin. Med. 2 (3) (2019) 152–165.
[37] M. Uhlén, et al., Proteomics. Tissue-based map of the human proteome, Science (1979) 347 (6220) (2015) 1260419.
[38] K. Murakami, N. Umemura, M. Adachi, M. Motoki, E. Ohkoshi, ABCG2, CD44 and SOX9 are increased with the acquisition of drug resistance and involved in cancer stem cell activities in head and neck squamous cell carcinoma cells, Exp. Ther. Med. 24 (6) (2022) 722.
[39] N. Sheng, et al., SOX9 promotes stemness in the CAL27 cell line of tongue squamous cell carcinoma, Cell Biochem. Funct. 42 (3) (2024) e4000.
[40] S. Barbosa, et al., The role of SOX2 and SOX9 in radioresistance and tumor recurrence, Cancers (Basel) 16 (2) (2024) 439.
[41] E.E. Wicks, G.L. Semenza, Hypoxia-inducible factors: cancer progression and clinical translation, J. Clin. Invest. 132 (11) (2022) e159839.
[42] H.J. Lee, et al., Role of HIF1α regulatory factors in stem cells, Int. J. Stem Cells 12 (1) (2019) 8–20.
[43] M.G. Vasconcelos, et al., Distribution of hypoxia-inducible factor-1α and glucose transporter-1 in human tongue cancers, J. Oral Maxillofac. Surg. 73 (9) (2015) 1753–1760. *: official journal of the American Association of Oral and Maxillofacial Surgeons*.
[44] M. Ribeiro, et al., Expression of hypoxia-induced factor-1 alpha in early-stage and in metastatic oral squamous cell carcinoma, Tumour Biol. 39 (4) (2017) 1010428317695527. *: the journal of the International Society for Oncodevelopmental Biology and Medicine*.
[45] A.W. Eckert, M. Kappler, I. Große, C. Wickenhauser, B. Seliger, Current understanding of the HIF-1-dependent metabolism in oral squamous cell carcinoma, Int. J. Mol. Sci. 21 (17) (2020) 6083.
[46] X. Zhou, et al., Effect of HIF-1α on biological activation of human tongue squamous cell carcinoma SCC-15 cells in vitro, Int. J. Oncol. 46 (6) (2015) 2346–2354.
[47] Y. Hu, Y. Han, M. He, Y. Zhang, X. Zou, S100 proteins in head and neck squamous cell carcinoma (Review), Oncol. Lett. 26 (2) (2023) 362.
[48] Z. Huang, et al., Silencing LCN2 suppresses oral squamous cell carcinoma progression by reducing EGFR signal activation and recycling, J. Exp. Clin. Cancer Res. CR 42 (1) (2023) 60.
[49] M. Liu, et al., Identification of the MMP family as therapeutic targets and prognostic biomarkers in the microenvironment of head and neck squamous cell carcinoma, J. Transl. Med. 21 (1) (2023) 208.
[50] C.Y. Hsieh, et al., Macrophage secretory IL-1β promotes docetaxel resistance in head and neck squamous carcinoma via SOD2/CAT-ICAM1 signaling, JCI Insight. 7 (23) (2022) e157285.
[51] A.M. Urvalek, et al., Identification of ethanol and 4-nitroquinoline-1-oxide induced epigenetic and oxidative stress markers during oral cavity carcinogenesis, Alcohol Clin. Exp. Res. 39 (8) (2015) 1360–1372.
[52] R. Masood, et al., A novel orthotopic mouse model of head and neck cancer and lymph node metastasis, Oncogenesis 2 (9) (2013) e68.
[53] M. Hu, B. Tang, Y. Dai, X. Zhao, Unveiling the regulatory mechanism of nimotuzumab on PD-L1 expression in head and neck squamous cell carcinoma patients: implications for enhanced anticancer treatment strategies, Cell Signal 121 (2024) 111290.
[54] V.L. Dengler, M. Galbraith, J.M. Espinosa, Transcriptional regulation by hypoxia inducible factors, Crit. Rev. Biochem. Mol. Biol. 49 (1) (2014) 1–15.
[55] S. Na, et al., Plumbagin-mediating GLUT1 suppresses the growth of human tongue squamous cell carcinoma, Oral Dis. 24 (6) (2018) 920–929.
[56] A. Kumari, et al., Role and regulation of GLUT1/3 during oral cancer progression and therapy resistance, Arch. Oral Biol. 150 (2023) 105688.
[57] A. Kita, et al., Activin B regulates adhesion, invasiveness, and migratory activities in oral cancer: a potential biomarker for metastasis, J. Cancer 8 (11) (2017) 2033–2041.
[58] L.K. Dionne, E.R. Driver, X.J. Wang, Head and neck cancer stem cells: from identification to tumor immune network, J. Dent. Res. 94 (11) (2015) 1524–1531.
[59] S. Raj, A. Kumar, D. Kumar, Regulation of glycolysis in head and neck cancer, Adv. Exp. Med. Biol. 1280 (2021) 219–230.
[60] Q. Wang, et al., Pharmacological inhibition of Bmi1 by PTC-209 impaired tumor growth in head neck squamous cell carcinoma, Cancer Cell Int. 17 (2017) 107.
[61] T. Ohashi, K. Terazawa, H. Shibata, N. Inoue, T. Ogawa, Metabolic profiling analysis of head and neck squamous cell carcinoma, Oral Dis. 30 (2) (2024) 342–352.
[62] J. Liang, et al., Rac1 promotes the reprogramming of glucose metabolism and the growth of colon cancer cells through upregulating SOX9, Cancer Sci. 114 (3) (2023) 822–836.
[63] S. Ohba, X. He, H. Hojo, A.P. McMahon, Distinct transcriptional programs underlie SOX9 regulation of the mammalian chondrocyte, Cell Rep. 12 (2) (2015) 229–243.
[64] M. Rahmoun, et al., In mammalian foetal testes, SOX9 regulates expression of its target genes by binding to genomic regions with conserved signatures, Nucl. Acids Res. 45 (12) (2017) 7191–7211.
[65] X.H. Tang, M. Albert, T. Scognamiglio, L.J. Gudas, A DNA methyltransferase inhibitor and all-trans retinoic acid reduce oral cavity carcinogenesis induced by the carcinogen 4-nitroquinoline 1-oxide, Cancer Prevent. Res. 2 (12) (2009) 1100–1110.
[66] X.H. Tang, et al., Combination of bexarotene and the retinoid CD1530 reduces murine oral-cavity carcinogenesis induced by the carcinogen 4-nitroquinoline 1-oxide, Proc. Natl. Acad. Sci. U.S.A. 111 (24) (2014) 8907–8912.
[67] K. Osei-Sarfo, X.H. Tang, A.M. Urvalek, T. Scognamiglio, L.J. Gudas, The molecular features of tongue epithelium treated with the carcinogen 4-nitroquinoline-1-oxide and alcohol as a model for HNSCC, Carcinogenesis 34 (11) (2013) 2673–2681.
[68] X.H. Tang, A retinoic acid receptor β2 agonist attenuates transcriptome and metabolome changes underlying nonalcohol-associated fatty liver disease, J. Biol. Chem. 297 (6) (2021) 101331.
[69] D. Torre, A. Lachmann, A. Ma'ayan, BioJupies: automated generation of interactive notebooks for RNA-seq data analysis in the cloud, Cell Syst. 7 (5) (2018) 556–561, e553.